ICSO 2016

International Conference on Space Optics

Biarritz, France

18–21 October 2016

Edited by Bruno Cugny, Nikos Karafolas and Zoran Sodnik

Design and manufacturing of a compact two-mirror system for multispectral imaging applications

G. Vecchi

S. Basso

E. Buratti

M. Civitani

et al.

International Conference on Space Optics — ICSO 2016, edited by Bruno Cugny, Nikos Karafolas, Zoran Sodnik, Proc. of SPIE Vol. 10562, 1056254 · © 2016 ESA and CNES
CCC code: 0277-786X/17/$18 · doi: 10.1117/12.2296124

DESIGN AND MANUFACTURING OF A COMPACT TWO-MIRROR SYSTEM FOR MULTISPECTRAL IMAGING APPLICATIONS

G. Vecchi[1], S. Basso[1], E. Buratti, M. Civitani[1], P. Conconi[1], M. Ghigo[1], J. Hołyszko[1], G. Pareschi[1], G. Sironi[1] and G. Tagliaferri[1]
[1]INAF/Brera Astronomical Observatory, Via E. Bianchi 46, 23807 Merate (LC), Italy

I. INTRODUCTION

Spectral imaging systems drive the development of remote sensing applications. The possibility to combine integrated multispectral sensors to compact, broadband and wide field optical systems is highly advantageous in terms of reliability, portability, and cost reduction. On the other hand, such optical systems often rely on the feasibility of demanding optical components, as of strongly aspheric optics. The activity of manufacturing and metrological testing of such optics is crucial for the achievement of the whole project. In this paper, we present the design of a compact two-mirror system and the manufacturing of the strongly aspheric primary mirror.

II. DESIGN OF THE OPTICAL SYSTEM

We designed a broadband and wide field optical system that enables multispectral imaging in a reflective configuration. After an assessment of previous projects, we found an alternative solution to the three or four mirror telescopes for spectral imaging applications [1-2]. Our solution consists in a very compact two-mirror telescope, designed to meet the strict payload requirements for airborne remote sensing of environment. The overall system needs to be included into a maximum volume of 200 x 200 x 300 mm^3, which is the volume allowance for payloads onboard the C-100 Vulcan, an ultralight aircraft considered as baseline aerial platform for the project. In parallel to the volume constraint, we optimized the weight of the telescope, by designing the rigid structure that supports and integrates the optics and the imaging sensor systems. Concerning the spectral performance, the purpose was to permit the system of optics and detector to operate over a wide spectrum from visible to long wavelength infrared. We wanted an optical system with a large field of view and good spatial resolution, limited only by the pixel size of the detector.
Therefore, we fixed a few requirements in order to finalize our optical design, schematically shown in Fig. 1A. We assumed a detector made of 512 x 512 pixels, with pixel size of 50 µm; we considered the VIS-NIR spectral band; we assumed the volume prescription for the Vulcan platform, and a field of view of 6.4 x 6.4 deg^2. We have fulfilled such prescriptions with a very compact configuration, made of only two aspheric mirrors. Omitting a third mirror comes at the price of a more challenging manufacturing of the mirrors, particularly of the primary mirror, which displays a larger aspheric departure than in a three-mirror design. Moreover, we performed a trade-off analysis between two possible configurations of the two-mirror solution. In one configuration, the focal plane is set between the mirrors, and this leads to a stringent limit for the volume assigned to the detector system. The second option has the focal plane behind the primary mirror, as represented in Fig. 1A. We finally selected this second option as the baseline for the project. Fig.1B reports on-axis and off-axis images of a point-like source.

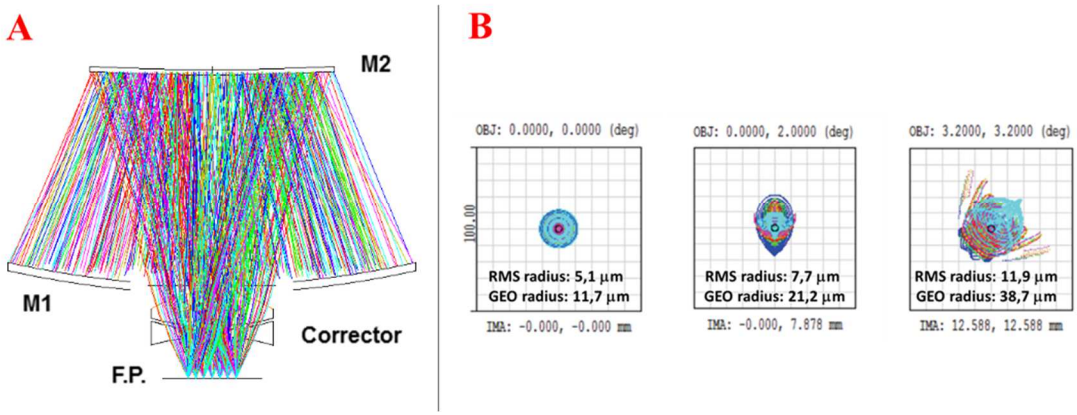

Fig. 1. A. Layout of the optical design, with field corrector for VIS-NIR. B. Spot diagrams.

Both mirrors are aspheric and the primary deploys the largest aspheric departure from the best-fit sphere, close to 460 µm, as shown in Fig. 2.

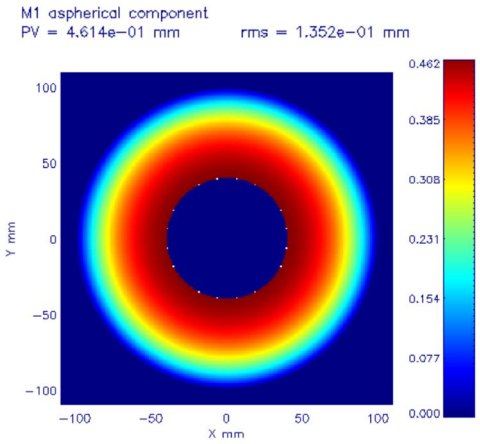

Fig. 2. Aspherical component of the primary mirror.

For this preliminary design, we considered a field flattener operating in the 0.4-4 µm spectral range, also providing a window in front of the detector. However, we assessed the feasibility of a more complex corrector operating over an extended range from visible up to 10 µm. We estimated acceptable the decrease in the optical throughput of the overall telescope caused by this corrector, a reduction similar to having a third mirror in the system.
The choice of a simplified design implied an increased challenge from the viewpoint of manufacturing. In consideration of a few features of the primary mirror, the highest degree of asphericity, the size, and the need for hollowing it, we recognized its manufacturing as a stepping-stone for the follow-up of the whole project. Therefore, we have adopted this primary mirror as bench test for our under development manufacturing capability.

III. FINITE ELEMENT ANALYSIS

Starting from the optical design described above, we designed a structure to integrate the optics, i.e., mirrors and field corrector, and the detector into a system fulfilling the volume and weight requirements. Modal analysis to identify resonance frequencies of the system provided promising results. We calculated the lowest resonant frequency at 179 Hz associated with the rotation around the axis of the secondary mirror. Such value is sufficiently decoupled from the natural frequencies associated to the aircraft body near the telescope, evaluated below 50 Hz.
We conducted a study based on finite element method (FEM) to analyze the thermo-mechanical loads and, therefore, to select the most suitable materials to make both the optical and the mechanical sub-systems. In Fig. 3, we show the FEM model for the entire structure. The different colors indicate different materials, as listed in the Table.

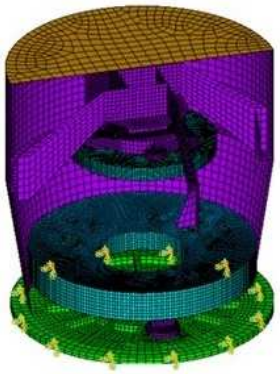

	Mass [kg]	Material
Assembly Tube	1.64	Invar
Blades	0.13	Invar
Interface Plate	1.07	Titanium
M2	0.44	Zerodur
M2 Spider	1.10	Invar
M2 Frame	0.34	Invar
Primary Mirror	1.45	Zerodur
Camera (and supports)	1.50	n.a.
Cover	0.94	Fused Silica
Total	8.61	

Fig. 3. FEM model of the structure. Different colors refer to the different materials in the list.

We have selected Zerodur as the material for the two mirrors, Titanium for the interface plate of the system to the aircraft platform. Assembly tube, blades and the supporting frame for the secondary mirror (M2) should use Invar for its excellent thermal characteristics. In the Table, we also display the mass calculated for every element of the system: the total weight is compliant with the requirement of max 9 Kg allowed for the payload.

IV. MANUFACTURING OF THE PRIMARY MIRROR

A. Grinding phase

Zerodur is a glass ceramic material produced by SCHOTT, characterized by an extreme thermal stability, a property that makes it an excellent choice to minimize any figure deformation induced by thermal gradients. Zerodur has also another important property in the ease of manufacturability. Machining Zerodur blanks with numerical control grinding processes is possible to high levels of precision. Particularly, Zerodur surfaces are suitable for polishing to high quality standards.

We report on the procurement and manufacturing of the 200 mm f/1.1 primary mirror, concave and with on-axis aspheric shape.

We procured a disc of Zerodur with diameter of 200 +1/-0 mm and thickness of 27.0 ± 0.5 mm. We outsourced the grinding, with the goal in this phase to approximate the nominal shape of the surface with a tolerance on the form error of 7 µm PV. During this step of the manufacturing activity, we have also perforated the center of the disc with a hole of 80 mm diameter. The hole will allow the light bounced back from the secondary mirror to reach the detector at the focal plane. We could have postponed the primary hollowing after the polishing phase. However, we decided not to risk of damaging the mirror after it, because of its higher added value.

Fig. 4A shows the mirror after the grinding and hollowing phase, mounted into an aluminum support, which we designed and manufactured in our workshop to provide a common interface plate to the polishing machine and to the metrology setups. Fig. 4B shows the mirror under characterization by the optical profilometer [3] after the grinding. At this stage, the surface was not yet of optical grade and appeared opaque. Roughness was evaluated by measuring the parameter Ra within the 0.25÷0.35 µm range. The non-contact sensor of the profilometer is working also on rough surfaces, allowing us to characterize unpolished surfaces of size up to about 200 mm. We measured the shape error of the mirror after grinding and we found a residual error of about 10 µm PV from the theoretical shape, taking into account the nominal best-fit sphere whose radius of curvature is 422.1 mm.

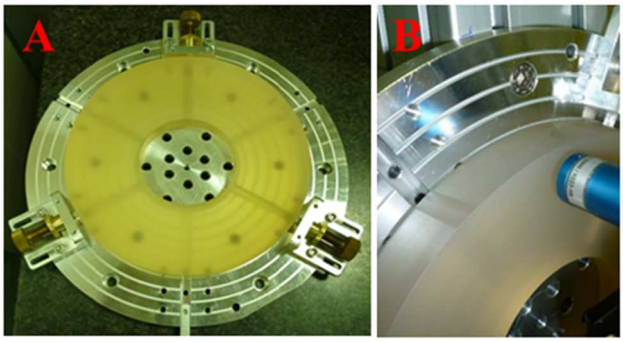

Fig. 4. A. Primary mirror received after grinding and mounted on the interface flange. B. Optical profilometry before polishing. The scanning non-contact sensor head is also visible.

B. Polishing technique

We used an IRP1200 machine (Intelligent Robotic Polisher) by Zeeko Ltd [4] to perform the polishing of the primary mirror. The machine, shown in Fig. 5A, is a robotic polisher that we installed in our labs in 2015. It allows the manufacturing of precision optics up to 1.2-meter diameter [5]. This computer-controlled system is equipped to apply either sub-aperture bonnet polishing or fluid jet polishing on a workpiece. Both options rely on the concept that the amount of material removed depends on the time the narrow jet (typically with size of a few mm) or the bonnet tool dwells at every position of the surface. The jet polishing removes material from the surface of a workpiece by projecting against it a high-speed fluid jet containing abrasive particles. For this project, the bonnet polishing has been developed and used, in which an inflated rubber tool or bonnet, covered with a layer of some kind of polishing felt, is pressed against the surface and is wet by a flux of abrasive slurry. A contact spot is defined between the bonnet and the surface of the workpiece. The spot size can range from about 5 mm up to a few tens of mm by replacing the bonnet, and is preserved throughout the polishing process. The contact spot dwells at every position for an amount of time calculated upon the measured map of residual error on the surface. In this way, the profile of a generic error map is progressively corrected, namely, moderated. Density of the slurry, pressure locally applied in the contact spot, rotation speed of the bonnet are among the main parameters that drive the removal rate for any specific material of workpiece. The spherically shaped bonnet falls in the category of compliant polishing tools. Therefore, it is capable to conform to the local aspherical shape of the generic workpiece, while it is poorly or not effective in smoothing out the mid-spatial error components, with wavelength shorter than the spot size in the millimeter range. Correcting the form error

in this frequency range can occur by applying less compliant tools, such as pitch pads, and customizing the relative processes. The task of addressing the error map in the mid-spatial frequency range remains challenging as regards to strongly aspheric optics [6].
Fig. 5B shows the primary mirror under polishing. The cerium-oxide slurry is pumped into the system at constant temperature, delivered by nozzles to the workpiece and is recirculated through a pipe drain. The abrasive slurry easily flushes through the hole in the mirror, while the interface plate was also devised with holes and radial channels to help draining it.

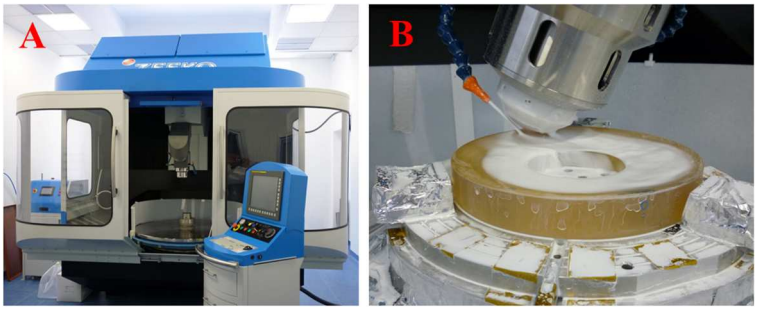

Fig. 5. A. IRP1200 series machine in the clean room. The slurry management unit is on the left of the machine. B. Primary mirror during the polishing run.

C. Interferometric test

We realized an interferometric setup to test the primary mirror during the progress of the figuring and polishing process. The setup is shown in Fig. 6A and is composed of three main elements: the tip-tilt holder for the mirror, the Zygo GPI series Fizeau interferometer, and an aluminum-based lens-tube assembly including a set of three N-BK7 lenses. The instrument was equipped with a 4-inch f/3.3 transmission sphere, therefore, not fast enough to cover the mirror aperture fully. To overcome this limitation, we procured a set of two high-performance (λ/20 PV each surface) lenses designed to modify the aperture of the wavefront from f/3.3 to f/1.1, matching the f-number of the primary mirror. The third optical element inserted in the beam path is visible in Fig. 6A, mounted at the edge of the lens assembly, and is the null corrector that enables the test of the aspherical mirror. We procured the null lens with 160 mm diameter and with surface irregularity of λ/4 PV.
The first run of polishing brought the surface of the mirror to a quality eligible for the interferometric test, and Fig. 6B displays the fringe pattern measured at that stage.

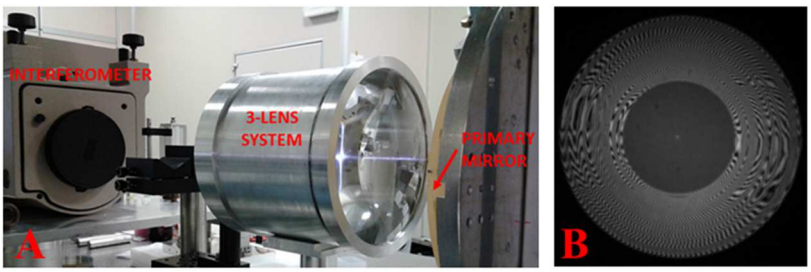

Fig. 6. A. View of the setup for the interferometric test. B. Fringe pattern after the first polishing run.

D. Polishing in progress

The pattern of interferometric fringes shown in Fig. 6B shows several ring features, associated to regions where the high number of fringes hinders the measurement. Therefore, with the applied setting, the interferometric setup could not provide an accurate measurement of the residual error spanning over the whole surface.
We think that the origin of the ring features is due to the grinding process of the workpiece. At this stage, we applied optical profilometry, as shown in Fig. 4B, to try to circumvent the problem found with interferometry. By rastering the head sensor through the surface, we aimed to map the ring features on it. The high spatial resolution needed meant tens of hour's long scans; moreover, the error maps were affected by the limited accuracy of our profilometer when measuring steep surface slopes, as in this case. However, we were able in this way to circumvent the issue and we could start the iterative process by applying the bonnet corrective polishing.
A few process iteration targeted the reduction of the rings amplitude, to let the whole surface becoming measurable with the interferometric setup. We proceeded with the moderation process up to meeting the form

irregularity tolerance devised by the optical project, λ/2 PV. This tolerance applies within the clear aperture of the primary mirror, which we assumed ranging from 105 up to 180 mm diameters. Due to the obscuration expected near the inner edge, introduced by a secondary mirror sized to 120 mm diameter in the baseline design, we did not focus on the accurate figuring of the edges at this stage of the project. Polishing techniques with a sub-aperture contact spot are known to be less reliable when it comes to address the near edge zones of optical parts. We therefore plan to target this aspect by taking advantage of another technology mastered in our labs, the ion beam figuring, where the sub-aperture tool has no mechanical contact to the workpiece [7].
In Fig. 7A we show the fringe pattern measured after a series of form corrective runs. The iterative moderation process has reduced the ring amplitude by an order of magnitude, from a few microns to a few hundreds of nanometers. Fig. 7B shows the corresponding residual error map measured in the clear aperture, with tilt and power terms removed. Most of the 350 nm PV is related to the residual pattern of grinding rings. The following run has further reduced the ring amplitude, as reported in Fig. 7C. The graph displays two profiles, extracted out of contour maps measured after the two last iterations. To help monitor the ring amplitude evolution, we also removed other low-order aberration terms, astigmatism and coma. This is because, at this level of form accuracy, we have noticed that the procedure of alignment between the mirror and the null lens tube is affecting the reproducibility of the measurement. The whole ring pattern has reached close to 200 nm PV.

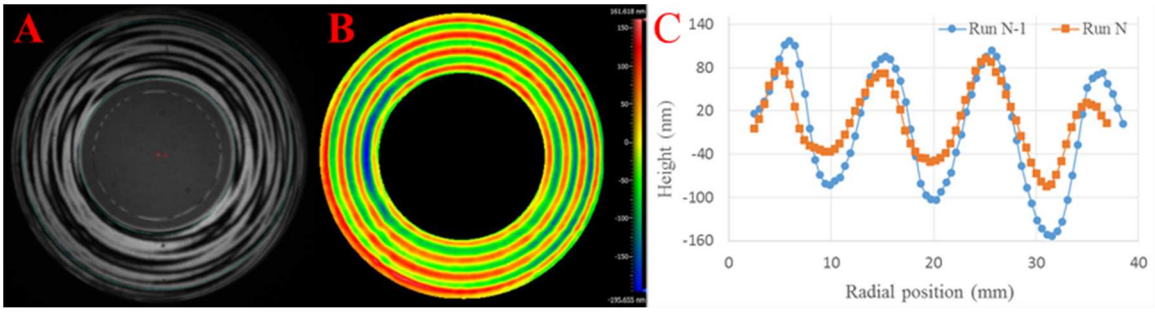

Fig. 7. A. Fringe pattern after corrective polishing. B. Corresponding error contour map in the 105-180 mm clear aperture. Tilt and power terms were removed. C. Radial profiles from residual error maps (tilt, power, astigmatism and coma were removed) after the two last iterations of polishing.

Further improvement of the form error accuracy is envisageable in two ways. One is to proceed by applying the ion beam figuring technique. The other way would consist in applying the corrective polishing by taking into account the detailed influence function defined at the contact spot.

V. RESULTS

Fig. 8 shows the spot diagrams obtained for the VIS range by applying the ray tracing code and taking into account the residual form error map of the primary mirror.

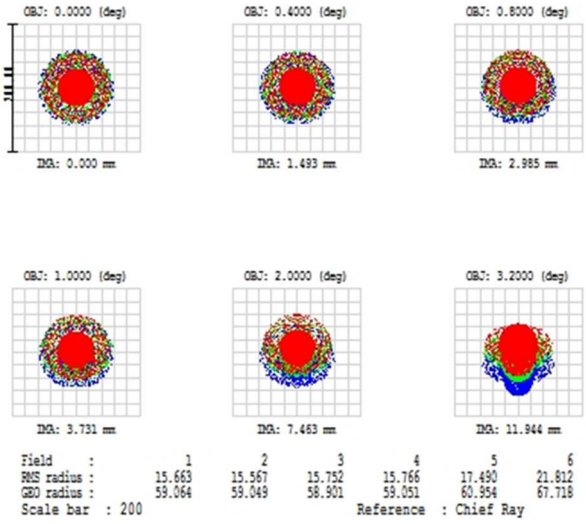

Fig. 8. Spot diagrams for the VIS range.

In Fig. 9, we plot the encircled energy falling into one detector's pixel with size of 50 µm for wavelength in the VIS range. We observe that up to 90% of the energy falls into such a pixel and this is true up to 2 deg off-axis. The figure reduces to 80% near the edge of the field of view. Therefore, the system is compliant with the requirement of having 80% of energy in the visible range within one pixel.

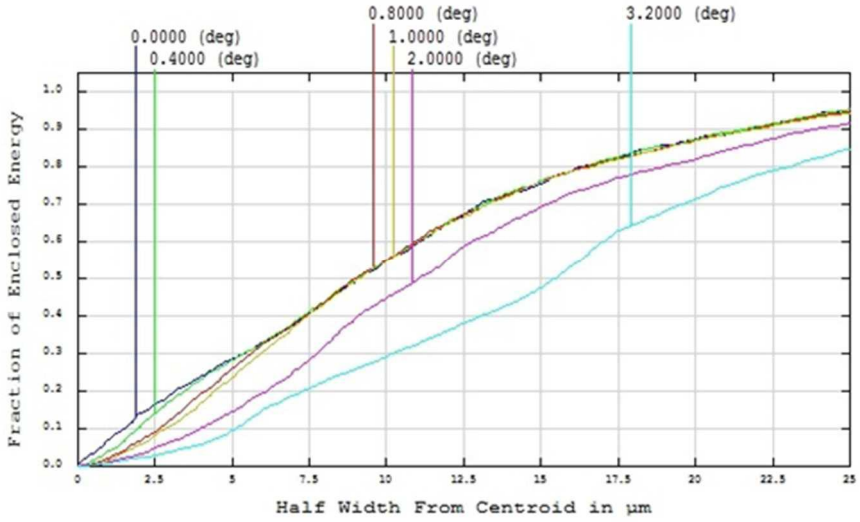

Fig. 9. Encircled energy as a function of pixel size for wavelength in the VIS range.

In Fig. 10, we display the Point Spread Function calculated at a wavelength of 3 µm with the Huygens method. The value 0.79 obtained for the Strehl ratio indicates the good quality achieved by the system in the infrared despite the residual presence of the ring pattern in the primary mirror.

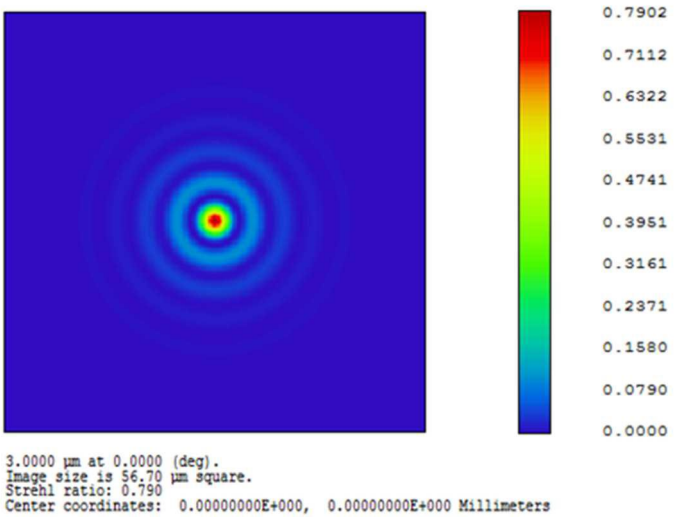

Fig. 10. Point Spread Function calculated at a wavelength of 3 µm.

VI. CONCLUSIONS

We have presented the design of a two-mirror telescope aimed for multispectral imaging in remote sensing applications. The telescope is very compact owing to the selection of strongly aspheric mirror surfaces. We performed design and FEM analysis of the whole telescope opto-mechanical structure, fulfilling both volume and weight requirements for the integration onto an airborne platform. We selected the primary mirror as the technological demonstrator of our manufacturing capability. We procured the mirror blank in Zerodur, and we have iterated the process of form correction by bonnet polishing up to achieving the initially targeted surface irregularity, near λ/2 PV. We monitored the evolution of surface accuracy by measuring it with an interferometric test setup. Spot diagrams, encircled energy and Strehl ratio calculations confirm that the achieved quality of the primary mirror is in line with the design requirements. To improve further the form error

accuracy we will apply ion beam figuring. Another possibility is to include the details of the influence function when applying the form corrective polishing.

REFERENCES

[1] M. Rossi, G. Borghi, I. A. Neil, G. Valsecchi, P. Zago, and F. E. Zocchi, "Electroformed off-axis toroidal aspheric three-mirror anastigmat multispectral imaging system", *Opt. Eng.*, vol. 53 (3), 031308, 2014.
[2] P. Gloesener, F. Wolfs, F. Lemagne, M. Cola, C. Flebus, G. Blanchard, and V. Kirschner, "Design, manufacturing and testing of a four-mirror telescope with a wide field of view", *ICSO Proceedings*, 2010.
[3] M. Civitani, M. Ghigo, O. Citterio, P. Conconi, D. Spiga, G. Pareschi, and L. Proserpio, "3D characterization of thin glass x-ray mirrors via optical profilometry", *Proc. of SPIE*, vol. 7803, 78030L, 2010.
[4] http://www.zeeko.co.uk/site/tiki-index.php.
[5] G. Vecchi, S. Basso, M. Civitani, M. Ghigo, G. Pareschi, M. Riva, and F. M. Zerbi, "A bonnet and fluid jet polishing facility for optics fabrication related to the E-ELT", *Mem. S.A.It.*, vol. 86 n. 3, 408, 2015.
[6] Z. Jian, "Bonnet Polishing High-Slope Aspheric Surface", *Proc. of SPIE*, vol. 8416, 841612, 2012.
[7] M. Ghigo, G. Vecchi, S. Basso, O. Citterio, M. Civitani, E. Mattaini, G. Pareschi, G. Sironi, "Ion figuring of large prototype mirror segments for the E-ELT", *Proc. of SPIE*, vol. 9151, 91510Q, 2014.